Published in: *Encyclopedia of Atmospheric Sciences*
Edited by J. R. Holton, J. Pyle, and J. A. Curry
Academic Press, San Diego (2003), pp. 1882–1891

The .pdf version of this chapter is available on-line at
http://www.giss.nasa.gov/~crmim/publications/

RADIATIVE TRANSFER / Scattering

M Mishchenko, L Travis and A Lacis, Goddard Institute for Space Studies, New York, NY, USA

Introduction

A parallel beam of light, or of any electromagnetic radiation, propagates in a vacuum without a change in its characteristics. However, interposing a particle into the beam causes several distinct effects. First, the particle may convert some of the energy contained in the beam into other forms of energy such as heat. This phenomenon is called absorption. Second, it scatters some of the incident energy in all directions at the same frequency. This phenomenon is called elastic

scattering. The energy of the incident beam is accordingly reduced by the amount equal to the sum of the absorbed and scattered energy. This reduction is called extinction.

The electromagnetic interaction becomes more complicated for a cloud of particles in the beam, because now each particle is illuminated not only by the external source but also by light scattered by all other particles. As a consequence, the light reflected or transmitted by the cloud of particles is multiply scattered.

The single-scattering and absorption characteristics of an isolated particle may be complicated functions of the particle size, morphology, and composition and can be determined by solving theoretically the Maxwell equations or by using one of the available experimental techniques. The process of multiple light scattering by clouds of particles is described by the radiative transfer equation subject to appropriate boundary conditions.

Sunlight incident on the Earth's atmosphere is scattered by gas molecules and suspended particles, giving rise to blue skies, white clouds, and various optical displays such as rainbows, halos, and the glory. By scattering and absorbing the incident short-wave solar radiation and the long-wave radiation emitted by the underlying surface, cloud and aerosol particles strongly affect the Earth's radiation budget. As a consequence of the dependence of single-scattering characteristics on particle size, morphology, and composition, scattered light can be remarkably rich in implicit information on particle properties and thus provides a sensitive tool for remote analyses of clouds and aerosols.

Basic Single-Scattering Characteristics

The treatment of light scattering in the atmosphere is naturally separated into three parts: single scattering by an individual particle; single scattering by a small volume element containing a tenuous particle collection; and multiple scattering by the entire atmosphere. It is assumed that within the small volume element, the particles are randomly distributed and separated by at least several times their radii, a condition that is met by aerosol and cloud particles suspended in the atmosphere.

Consider a parallel monochromatic beam of light illuminating an arbitrary particle (**Figure 1**). In the absence of the particle, a well-collimated detector facing the incident beam (detector 1 in **Figure 1**) would receive the amount of radiant energy per unit time equal to ΔSI, where I is the intensity of the beam (the rate of energy flow across a unit area normal to the direction of propagation) and ΔS is the detector area, whereas detector 2 would measure no signal. As a consequence of the electromagnetic interaction between the incident beam and the particle, the signal measured by detector 1 becomes $\Delta SI - C_{\text{ext}}I$, where C_{ext} is the particle extinction cross-section and $C_{\text{ext}}I$ describes the net reduction of the energy of the incident beam. The signal measured by detector 2 is $\Delta Sr^{-2}(\mathrm{d}C_{\text{sca}}/\mathrm{d}\Omega)I$, where $\mathrm{d}C_{\text{sca}}/\mathrm{d}\Omega$ is the differential scattering cross-section, r is the distance between the particle and the detector, and $(\mathrm{d}C_{\text{sca}}/\mathrm{d}\Omega)I$ is the amount of scattered energy per unit time per unit solid angle. Both C_{ext} and $\mathrm{d}C_{\text{sca}}/\mathrm{d}\Omega$ have the dimension of area and depend on the particle size, shape, refractive index, and orientation as well as on the wavelength of the incident light λ. The net effect of the particle on the signal measured by detector 1 is to reduce the illuminated detector area by 'casting a shadow' of area C_{ext}. While this geometrical interpretation of the extinction cross-section does not imply that C_{ext} is simply equal to the area G of the particle projection on the detector surface, it suggests the introduction of the dimensionless extinction efficiency factor by dividing the extinction cross-section by the geometrical cross-section: $Q_{\text{ext}} = C_{\text{ext}}/G$. The differential scattering cross-section describes the angular distribution of the scattered intensity and is a function of the scattering direction.

The total amount of energy scattered by the particle per unit time is computed by integrating over all scattering directions and is given by $C_{\text{sca}}I$, where C_{sca} given by eqn [1] is the total scattering cross section.

$$C_{\text{sca}} = \int_{4\pi} \mathrm{d}\Omega \, \frac{\mathrm{d}C_{\text{sca}}}{\mathrm{d}\Omega} \qquad [1]$$

The amount of energy absorbed by the particle per unit time is determined by subtracting the total scattered energy from the total energy extracted from the incident beam and is equal to $C_{\text{abs}}I$, where $C_{\text{abs}} = C_{\text{ext}} - C_{\text{sca}}$ is the absorption cross-section.

The single-scattering and absorption properties of a small volume element containing a representative distribution of particle sizes, shapes, orientations, and/or refractive indices are computed assuming that each particle scatters and absorbs the incident light in exactly the same way as if all other particles did not exist. Then the optical cross-sections of the volume element are obtained by summing up the respective characteristics of all constituent particles. For example, the extinction cross-section of a volume element containing N particles is $\sum_{n=1}^{N} C_{\text{ext},n} = N\langle C_{\text{ext}}\rangle$, where the index n numbers the particles and $\langle C_{\text{ext}}\rangle$ is the ensemble-averaged extinction cross-section per

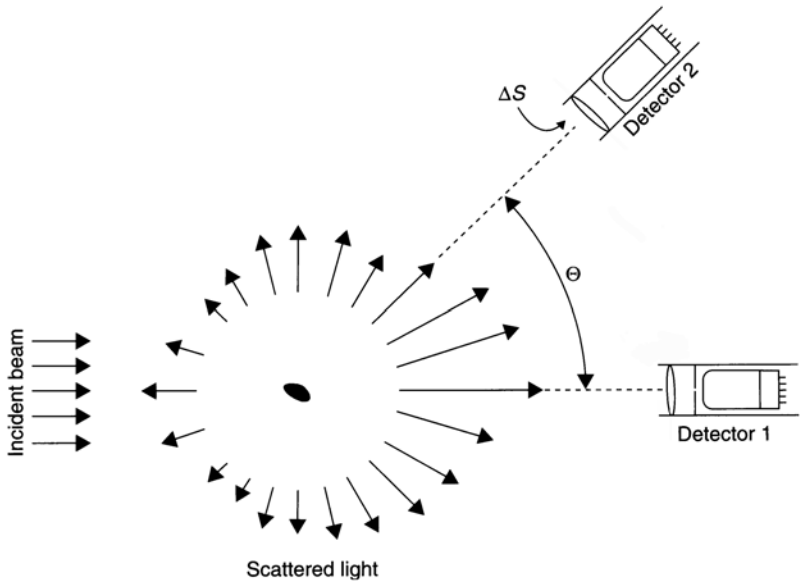

Figure 1 Response of a collimated detector depends on the line of sight.

particle. The extinction efficiency factor is now defined as $Q_{ext} = \langle C_{ext}\rangle/\langle G\rangle$, and similarly for Q_{sca} and Q_{abs}.

The dimensionless nonnegative quantity $\varpi = \langle C_{sca}\rangle/\langle C_{ext}\rangle$ is called the single-scattering albedo and is the ratio of the total scattered energy to the total energy extracted from the incident beam. ϖ is unity for nonabsorbing particles and is less than one for absorbing particles. The quantity $p = (4\pi/\langle C_{sca}\rangle)\langle dC_{sca}/d\Omega\rangle$ is called the phase function. As with the differential scattering cross-section, it describes the angular distribution of the scattered light, but is dimensionless and normalized (eqn [2]).

$$\frac{1}{4\pi}\int_{4\pi} d\Omega\, p = 1 \qquad [2]$$

The dimensionless asymmetry parameter [3] is defined as the cosine of the scattering angle Θ (the angle between the incidence and scattering directions in **Figure 1**) weighted by the phase function and averaged over all scattering directions.

$$\langle\cos\Theta\rangle = \frac{1}{4\pi}\int_{4\pi} d\Omega\, p\cos\Theta, \qquad -1 \le \langle\cos\Theta\rangle \le 1 \qquad [3]$$

The asymmetry parameter is positive if the particles scatter more light into the forward hemisphere ($\Theta < 90°$) is negative if more light is scattered into the backward hemisphere ($\Theta > 90°$), and is equal to zero if the scattering is symmetric with respect to the plane perpendicular to the incidence direction. $\langle\cos\Theta\rangle = 0$ for molecular scattering but is (significantly) greater than zero for most aerosol and cloud particles.

This simplified description of electromagnetic scattering is often called the scalar approximation because it ignores the vector nature of light. In reality, the beam of light must be characterized by a four-component Stokes column vector **I** with components I, Q, U, and V, of which the first is the intensity; the other three describe the polarization state of the beam (i.e., the characteristics of the preferential ellipse described by the endpoint of the electric field vector). All Stokes parameters have the dimension of energy flux. If detectors 1 and 2 in **Figure 1** were polarization-sensitive, they would measure the signals $\Delta S\mathbf{I} - \mathbf{KI}$ and $\Delta S r^{-2}\mathbf{FI}$, respectively, where **K** and **F** are 4×4 extinction and scattering matrices. Obviously, **F** describes the transformation of the Stokes vector of the incident beam into that of the scattered light. The 16 elements of the extinction and scattering matrices may all be nonzero, so the transmitted and scattered intensities may depend on all four Stokes parameters of the incident beam rather than only on its intensity. In particular, the fact that **K** does not transform to the scalar extinction cross-section for oriented nonspherical particles indicates that the particles can cause different attenuation rates for different polarization components of the incident beam, thereby changing the polarization state of the transmitted signal. This causes, for example, depolarization of radar signals propagating through precipitation. The scattered light

also has polarization characteristics different from those of the incident light, thereby making polarimetry a sensitive particle characterization technique. Despite its formal deficiency, the scalar approximation is often used when the incident light is unpolarized and only the intensity of the transmitted or scattered light is measured.

Computation and Measurement of Single-Scattering Characteristics

The evaluation of the Earth's radiation balance and analyses of remote sensing observations require accurate quantitative knowledge of the electromagnetic scattering interaction as a function of particle morphology and composition. This knowledge can be based on theoretical computations or experimental measurements, both approaches having their strengths and limitations. Theoretical modeling does not involve expensive instrumentation and allows switching to another particle shape, size, or refractive index by changing a few lines in a computer code. However, exact computations for realistic polydispersions of irregular particles are costly and are thus often replaced by computations for simplified shapes, whereas approximate calculations often have uncertain accuracy and range of applicability. Experimental measurements deal with real particles, but require complex and expensive hardware and may be difficult to interpret.

Theoretical Techniques

In electromagnetic terms, the parallel monochromatic beam of light is an oscillating plane electromagnetic wave, whereas the particle is an aggregation of a large number of elementary discrete electric charges. The oscillating electromagnetic field of the incident wave excites the charges to oscillate with the same frequency and thereby radiate secondary electromagnetic waves. The superposition of the secondary waves generated by all the charges gives the total scattered field. If the particle is absorbing, it scatters less total energy than it extracts from the incident wave.

Electromagnetic interaction is a complicated phenomenon because the secondary wave generated by each oscillating charge also stimulates oscillations of all other charges forming the particle and thus modifies their respective secondary waves. Because the number of elementary charges forming a micrometer-sized particle is extremely large, solving the scattering problem directly by computing and superposing all secondary waves can be a hopeless endeavor even with the aid of modern computers. Fortunately, the same problem can be handled using the concepts of macroscopic electromagnetics, which treat the large collection of charges as a macroscopic body with a specific distribution of the refractive index. The scattered field is then computed by solving the macroscopic Maxwell equations subject to appropriate boundary conditions. This approach is mathematically manageable and forms the basis of the modern theory of electromagnetic scattering by small particles.

All needs of a practitioner dealing with light scattering by spherical particles may be well served by the exact and highly efficient Lorenz–Mie theory which is the result of applying the separation of variables method to the vector wave equation in spherical coordinates. For nonspherical particles, exact computations must resort to more general and complex solutions traditionally divided into two broad categories. Differential equation methods compute the scattered field by solving the Maxwell or vector wave equations, subject to appropriate boundary conditions, in the frequency domain or in the time domain. Integral equation methods are based on the volume or surface integral counterparts of the Maxwell equations; the boundary conditions are included in the solution automatically.

The practical importance of approximate treatments of light scattering diminishes as various exact techniques mature and become applicable to a wider range of problems and computers become ever more powerful. However, at least one approximation is likely never to become obsolete because its accuracy only improves as the ratio of the particle size to the wavelength grows, while exact theoretical techniques for nonspherical particles cease to be practical whenever the ratio exceeds a certain threshold. This so-called geometrical optics approximation assumes that the particle size is much larger than the wavelength of the incident light and that the incident plane wave can be represented as a collection of independent parallel rays. The history of each ray impinging on the particle surface is traced using Snell's law and Fresnel formulas (**Figure 2**). Sampling all escaping rays into predefined narrow angular bins yields a quantitative representation of the particle scattering and absorption properties. The ray-tracing pattern is supplemented by the computation of Fraunhofer diffraction of the incident wave on the particle projection.

Measurements

Detectors of visible and infrared light are usually polarization-insensitive so that the detector response is determined only by the first Stokes parameter of the beam striking the detector. In order to measure all

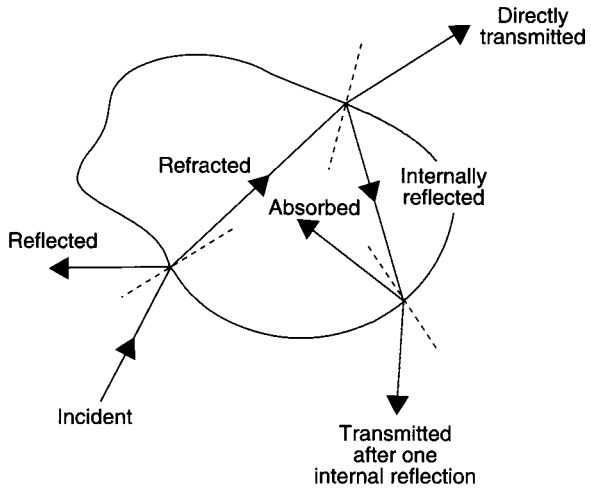

Figure 2 Ray-tracing diagram.

elements of the scattering matrix, one must insert into the beam various optical elements that can vary the polarization state of light before and after scattering in a controllable way (**Figure 3**). The use of high-frequency sinusoidal modulation in time of the polarization of light before scattering combined with intensity normalization and followed by lock-in detection increases the measurement accuracy and yields several elements from only one detected signal. The measurement procedure is repeated at different scattering angles in order to determine the angular profile of the scattering matrix.

Scattering measurements using visible and infrared light benefit from the availability of sensitive detectors (photomultipliers and avalanche semiconductor photodiodes), intense sources of radiation (lasers), and high-quality optical elements. They involve relatively inexpensive and portable instrumentation and can be performed in the field nearly as well as in the laboratory. However, they often suffer from poor advance knowledge of microphysical characteristics of scattering particles, thereby making difficult comparisons of experimental and theoretical results. The arrangement of the source of light and the detector precludes measurements at scattering angles close to 0° and 180°, which makes problematic the absolute measurement of the phase function (by enforcing the normalization of eqn [2]) and the total scattering cross-section.

Because particle size in the theoretical formulation of electromagnetic scattering is only encountered as a ratio to the wavelength, the main idea of the microwave analog technique is to manufacture a centimeter-sized scattering object with desired shape and refractive index, measure the scattering of a microwave beam by this object, and finally extrapolate the results to other wavelengths (e.g., visible or infrared) by keeping the ratio size/wavelength fixed (**Figure 4**). Microwave measurements allow a wide coverage of scattering

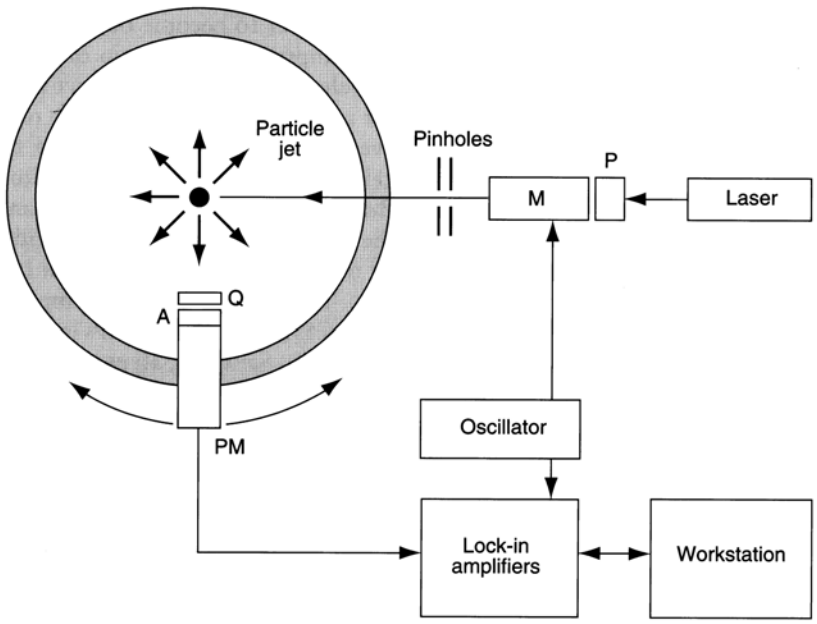

Figure 3 Schematic view of an experimental setup using visible or infrared light. The laser beam passes several optical elements before and after scattering and is detected by the photomultiplier. The latter is mounted on a circular rail and can be moved around the particle jet in order to cover a wide range of scattering angles. P, polarizer; A, polarization analyzer; Q, quarter-wave plate; PM, photomultiplier; M, electrooptic modulator.

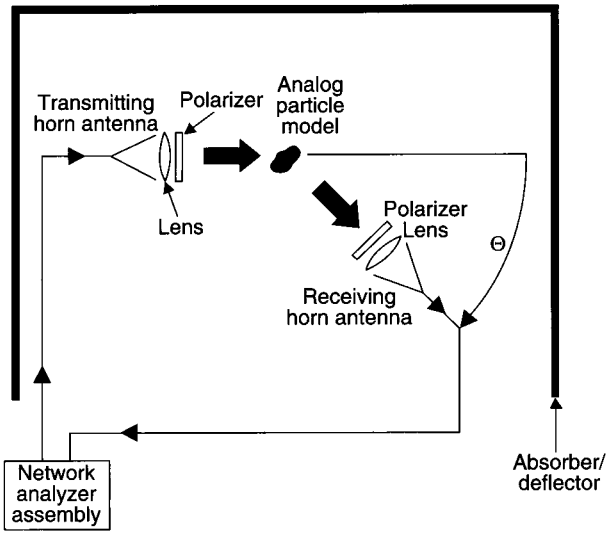

Figure 4 Layout of a microwave analog facility.

angles including the exact forward and backward directions and a much greater degree of control over the target size, shape, and orientation than do optical measurements. However, the microwave measurements require more cumbersome and expensive instrumentation and large measurement facilities. Furthermore, they are performed only for one particle size, shape, and orientation at a time, thereby making ensemble averaging a time-consuming process.

Multiple Scattering

Multiple scattering of light by the atmosphere containing sparsely and randomly distributed aerosol and cloud particles is usually described by the scalar radiative transfer equation (RTE) (eqn [4]).

$$\frac{dI(\hat{n})}{ds} = -n_0\langle C_{ext}\rangle I(\hat{n}) + \frac{n_0}{4\pi}\int_{4\pi} d\hat{n}'\langle C_{sca}\rangle p(\hat{n},\hat{n}')I(\hat{n}') \qquad [4]$$

$I(\hat{n})$ is the specific intensity of the multiply scattered light propagating in the direction $\hat{n}$ (i.e., the rate of energy flow per unit solid angle across a unit area normal to $\hat{n}$), the path length element ds is measured along $\hat{n}$, and n_0 is the local particle number density. The first term on the right-hand side of eqn [4] describes the decrease of the specific intensity caused by extinction over the distance ds, while the second term describes the increase of the specific intensity caused by scattering of light coming from all directions $\hat{n}'$ into the direction $\hat{n}$. The RTE must be supplemented by appropriate boundary conditions. For example, a standard model of the atmosphere is a multilayer plane-parallel system illuminated from above by solar radiation and bounded from below by a reflecting surface. The RTE can be solved numerically using various techniques such as the adding/doubling, discrete ordinate, and invariant imbedding methods. The scalar RTE is an approximation and must be replaced by the exact vector equation when one is specifically interested in the polarization characteristics of the scattered radiation.

Examples of Scattering by Clouds and Aerosols

The few examples following serve to illustrate some key features of electromagnetic scattering phenomena and their use in remote sensing of aerosols and clouds and radiation budget computations. **Figure 5** shows the scattering efficiency factor Q_{sca} versus size parameter for a narrow size distribution of spherical particles with refractive indices $m = 1.33$ and 1.45 (typical of water and sulfate aerosols at visible wavelengths, respectively). The size parameter is defined as $x = 2\pi r/\lambda$, where r is the effective radius of the size distribution. For wavelength-sized particles ($x \sim 5$), the scattering cross-section can exceed the particle geometrical cross section by a factor greater than 3.5. As the particle size becomes much larger, Q_{sca} tends to the asymptotic geometrical optics value of 2, with

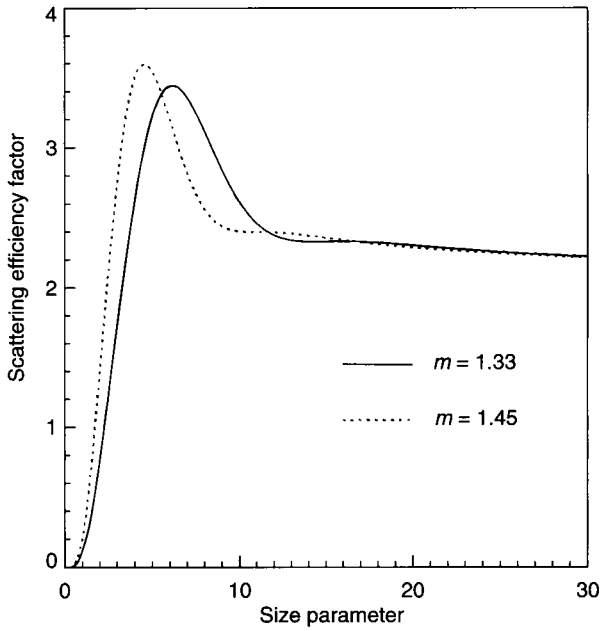

Figure 5 Scattering efficiency factor versus size parameter for polydisperse spherical particles with refractive indices (m) of 1.33 and 1.45.

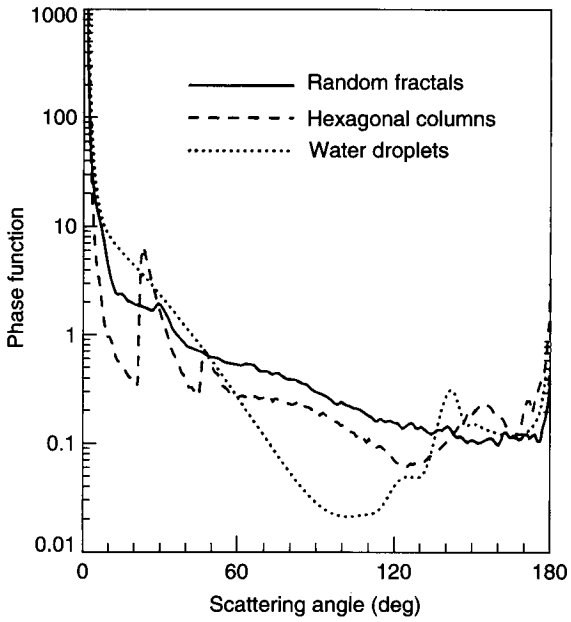

Figure 6 Phase functions for water cloud droplets, hexagonal ice columns, and randomly shaped ice crystals.

equal contributions from the rays striking the particle and the light diffracted by the particle projection. For particles much smaller than the wavelength, $Q_{sca} \propto \lambda^{-4}$, as first demonstrated by Lord Rayleigh and hence called Rayleigh scattering. Thus the scattering efficiency of gas molecules rapidly increases with decreasing wavelength, thereby explaining the blue color of skylight and the familiar reddening of the sunset.

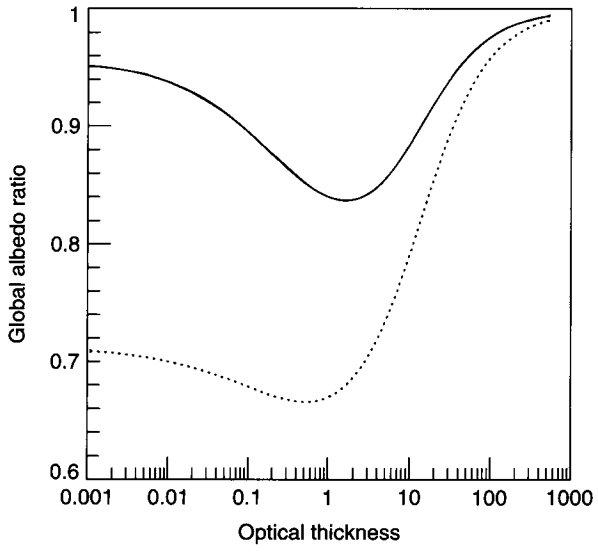

Figure 7 Global albedo of a liquid water cloud relative to that of an optical-thickness-equivalent ice cloud composed of irregular particles (dotted curve) and hexagonal columns (solid curve).

The dotted curve in **Figure 6** shows the phase function typical of spherical cloud droplets at visible wavelengths. The strong concentration of light at $\Theta = 0°$ is produced by Fraunhofer diffraction of light on the particle projection, whereas the feature at $\Theta \sim 140°$ is the primary rainbow generated by rays that have undergone only one internal reflection (**Figure 2**). The slight change of the rainbow angle with wavelength caused by dispersion gives rise to spectacularly colorful rainbows often observed during showers illuminated by the sun at an altitude lower than about 40°. The enhanced intensity at $\Theta \sim 180°$ is called the glory and can be seen from an airplane as a series of colored rings around the shadow cast by the airplane on the cloud top.

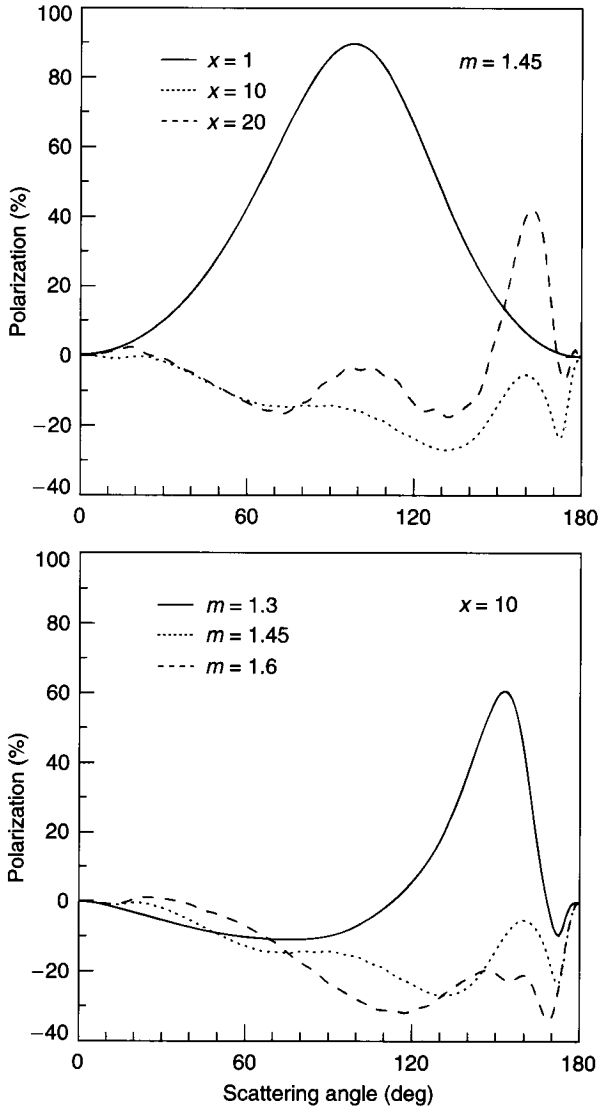

Figure 8 Linear polarization versus scattering angle for polydisperse spherical particles with varying size parameters $x(= 2\pi r/\lambda)$ and refractive indices m.

The dashed curve in **Figure 6** depicts the phase function typical of randomly oriented pristine hexagonal ice crystals. The concentrations of light at $\Theta \sim 22°$ and 46° are the primary and secondary halos attributed to minimum angles of deviation by 60° and 90° ice prisms. These features represent only two of many optical phenomena associated with regularly shaped ice crystals. Since cirrus clouds rather often fail to exhibit halos, the majority of real ice crystals appear to have highly irregular shapes and rough rather than flat surfaces. Such particles are better characterized by featureless phase functions like the one shown in **Figure 6** by the solid curve and computed for a random-fractal model of ice crystals.

Large numerical differences between the three phase functions depicted in **Figure 6** can cause significant differences in bidirectional reflectance of optical-thickness-equivalent water and ice clouds (optical thickness is defined as the average extinction cross-section per particle times the column particle number concentration). This, in turn, may lead to significant errors in the retrieved cloud optical thickness if remote-sensing reflectance measurements are inverted using an incorrect particle model. **Figure 7** illustrates

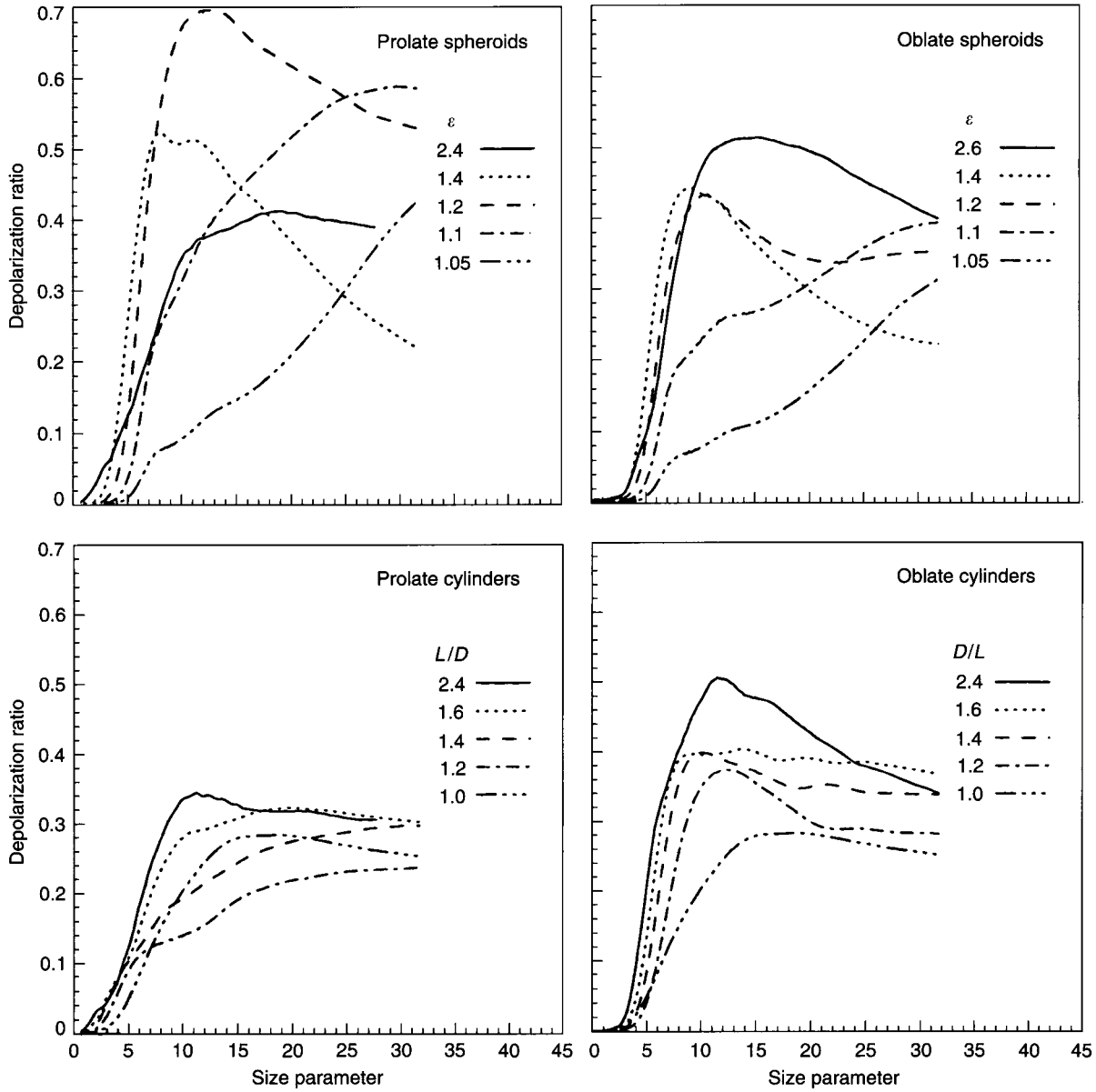

Figure 9 Depolarization ratio versus surface-equivalent-sphere size parameter for polydisperse, randomly oriented ice spheroids and cylinders. The refractive index is 1.311. ε is the ratio of the largest to the smallest semiaxes of a spheroid. The shapes of prolate and oblate cylinders are specified by length-to-diameter (L/D) and diameter-to-length (D/L) ratios, respectively.

the effect of particle shape on the global cloud albedo (defined as cloud reflectance averaged over all incidence and reflection directions) at visible wavelengths. The quantity (1 – cloud albedo) determines how much solar energy is absorbed or transmitted by the atmosphere and is an important climatological parameter. It is seen that for the same optical thickness, clouds composed of irregular ice crystals have the largest albedo, whereas those composed of water droplets are the least reflective. The explanation of this result is simple: the asymmetry parameter for the irregular ice crystals (0.752) is smaller than that for the hexagonal ice columns (0.816) and significantly smaller than that for the water droplets (0.862), thereby causing a larger fraction of the incident solar radiation to be backscattered and a smaller fraction to be scattered in the forward direction.

Figure 8 illustrates the ratio $P = -F_{12}/F_{11}$ of the scattering matrix elements (called the degree of linear polarization of the scattered light for unpolarized incident light) for polydisperse spheres with different refractive indices and size parameters. The obvious significant variability of polarization with m and r (or λ) makes it a very sensitive indicator of the particle physical properties. Furthermore, since P is a ratio of two intensities, it can be measured to a much greater precision than intensity. These two factors explain the remarkable potential of photopolarimetry as a remote sensing tool for aerosol and cloud particle characterization.

The fact that the Lorenz–Mie equality $F_{22}(180°) = F_{11}(180°)$ does not hold for nonspherical particles makes lidar and radar measurements of the depolarization ratio $\delta = [F_{11}(180°) - F_{22}(180°)]/[F_{11}(180°) + F_{22}(180°)]$ the most reliable detector of particle nonsphericity. **Figure 9** demonstrates δ for polydisperse, randomly oriented, nonspherical ice particles and shows that the growth of the size parameter from 0 to about 10 rapidly changes δ from 0 to large values sometimes approaching the theoretical limit $\delta_{max} = 1$. This property of the depolarization ratio makes it useful for sizing aerosol, cloud, and precipitation particles by performing multiwavelength measurements.

Notation

$\langle \cos\Theta \rangle$	asymmetry parameter of the phase function (dimensionless)
C_{abs}	absorption cross-section (m^2)
C_{ext}	extinction cross-section (m^2)
C_{sca}	scattering cross-section (m^2)
$dC_{sca}/d\Omega$	differential scattering cross section (m^2)
$\mathbf{F}$	scattering matrix (m^2)
F_{ij}	elements of the scattering matrix (m^2)
G	area of the particle geometrical projection (m^2)
I	intensity ($W\,m^{-2}$)
I	specific intensity ($W\,m^{-2}\,sr^{-1}$)
I	first Stokes parameter ($W\,m^{-2}$)
$\mathbf{I}$	4×1 Stokes vector ($W\,m^{-2}$)
m	refractive index (dimensionless)
$\hat{n}$	unit vector in the direction of propagation (dimensionless)
n_0	particle number density (m^{-3})
p	phase function (dimensionless)
P	degree of (linear) polarization (dimensionless)
Q	second Stokes parameter ($W\,m^{-2}$)
Q_{abs}	efficiency factor for absorption (dimensionless)
Q_{ext}	efficiency factor for extinction (dimensionless)
Q_{sca}	efficiency factor for scattering (dimensionless)
S	surface area (m^2)
U	third Stokes parameter ($W\,m^{-2}$)
V	fourth Stokes parameter ($W\,m^{-2}$)
δ	depolarization ratio (dimensionless)
Θ	scattering angle (radians)
$\mathbf{K}$	extinction matrix (m^2)
λ	wavelength (m)
ϖ	single-scattering albedo (dimensionless)
$\langle x \rangle$	average of x

See also

Aerosols: Role in Radiative Transfer. **Cloud Microphysics. Clouds:** Classification. **Contrails. Lidar:** Atmospheric Sounding Introduction. **Observations for Chemistry (Remote Sensing):** Lidar. **Radar:** Precipitation Radar. **Satellite Remote Sensing:** Aerosol Measurements.

Further Reading

Bohren CF and Huffman DR (1983) *Absorption and Scattering of Light by Small Particles*. New York: Wiley.

Chandrasekhar S (1960) *Radiative Transfer*. New York: Dover.

Coulson KL (1988) *Polarization and Intensity of Light in the Atmosphere*. Hampton, VA: Deepak.

Goody RM and Yung YL (1989) *Atmospheric Radiation*. New York: Oxford University Press.

Hansen JE and Travis LD (1974) Light scattering in planetary atmospheres. *Space Science Reviews* 16: 527–610.

Lenoble J (ed.) (1985) *Radiative Transfer in Scattering and Absorbing Atmospheres: Standard Computational Procedures*. Hampton, VA: Deepak.

Liou KN (1992) *Radiation and Cloud Processes in the Atmosphere*. New York: Oxford University Press.

Mishchenko MI, Hovenier JW and Travis LD (eds) (2000) *Light Scattering by Nonspherical Particles*. San Diego, CA: Academic Press.

Mishchenko MI, Travis LD and Lacis AA (2002) *Scattering, Absorption, and Emission of Light by Small Particles*. Cambridge: Cambridge University Press.

Stephens GL (1994) *Remote Sensing of the Lower Atmosphere*. New York: Oxford University Press.

Thomas GE and Stamnes K (1999) *Radiative Transfer in the Atmosphere and Ocean*. New York: Cambridge University Press.

van de Hulst HC (1957) *Light Scattering by Small Particles*. New York: Wiley.

van de Hulst HC (1980) *Multiple Light Scattering*. New York: Academic Press.